Numerical time-dependent Schroedinger description of charge-exchange collisions

Merle E. Riley* and Burke Ritchie**

*Sandia National Laboratories, Albuquerque, New Mexico 87185

**University of California, Lawrence Livermore National Laboratory, Livermore, California 94550

An implicit Fast Fourier Transform (FFT) algorithm is implemented to solve the time-dependent Schroedinger equation with application to charge-exchange collisions. Cross sections are calculated for He^{++} on H and compared with experiment and other theoretical results. A disagreement between previously published theoretical results is resolved.

DISCLAIMER

I. Introduction

The first work on the numerical solution of the time-dependent Schroedinger equation (TDSE) to describe charge-exchange collisions appeared nearly twenty years ago [1]. Computational limitations of this epoch meant that, except for head-on collisions, which are rotationally symmetric about the internuclear axis, one had to assume such symmetry in order to use an uncoupled 2D equation in cylindrical coordinates [1-4], although clearly for finite impact parameters rotational symmetry about the internuclear axis does not obtain. The problem is properly treated by expanding in eigen-states of the azimuthal quantum number, a procedure which generates a set of coupled 2D equations [5].

The partial differential equation (PDE) solver used in these calculations was the Peaceman-Rachford (PR) method [6], which is a generalization of the Crank-Nicolson method suitable for 2D problems. In general the description of charge-exchange requires a three-dimensional description, which necessitates the use of a 3D algorithm such as the split-operator fast Fourier transform (FFT) method [7]. Unfortunately this algorithm uses an explicit

temporal advance, leading to nonconservation of energy in Coulombic problems [8] except for values of the temporal increment dt which can turn out to be impractically small in a 3D numerical integration. Hence this method has historically been used in problems of a non-Coulombic nature which are found in optical and chemical physics. More recently other groups have used numerical methods to solve the TDSE [8,9].

In this paper we implement a 3D implicit split-operator procedure (ISOP) [10,11] for charge-exchange collisions. Implicit algorithms, in which the Hamiltonian is evaluated both at the advanced and retarded time steps, are more stable against numerical error than explicit algorithms, in which the Hamiltonian is evaluated only at the retarded time step. The present implicit method combines the computational speed of the explicit split-operator procedure (ESOP) method [7] with the numerical stability of the implicit 2D PR method [6]. In other words the implicit nature of the PR 2D method is achieved in 3D, thus ensuring the conservation of energy on a relatively coarse temporal grid [10], while at the same time all operations involving the Laplacian are carried out in

transform space, using standard FFT routines as in ESOP [7], thereby avoiding spatial differencing and matrix inversion operations.

II. Computational algorithm

Our computational algorithm consists of three operations carried out in succession for each temporal interval (where atomic units are used throughout),

$$(1 + \frac{dt}{8i}\nabla^2)\varphi = (1 - \frac{dt}{8i}\nabla^2)\psi_t \qquad (1a)$$

$$(1 - \frac{dt}{2i}V)\chi = (1 + \frac{dt}{2i}V)\varphi \qquad (1b)$$

$$(1 + \frac{dt}{8i}\nabla^2)\psi_{t+dt} = (1 - \frac{dt}{8i}\nabla^2)\chi \qquad (1c)$$

where the subscripts on the wave function refer to the solution at prior (t) and advanced (t+dt) time points. Operating on Eq. (1c) successively with the left-hand operators of Eqs. (1b) and (1a) and using Eqs. (1b) and (1a) to eliminate the intermediate functions χ and φ, we arrive at the net advancement algorithm,

$$(1 + \frac{dt}{4i}\nabla^2 - \frac{dt}{2i}V)\psi_{t+dt} = (1 - \frac{dt}{4i}\nabla^2 + \frac{dt}{2i}V)\psi_t + O(dt^3) \quad , \qquad (2)$$

which has the desired Crank-Nicolson form and is, as analysis shows, second-order accurate (hence our last term on the right side of Eq. (2) indicates that all other terms generated from the operations to eliminate the intermediate functions are of order dt^3 and can be dropped). It is not practical to use Eq. (2) directly except in 1D problems; therefore the algorithm is implemented using Eqs. (1), where the first and third steps are carried out in transform space using standard 3D FFT routines and the middle step is carried out in real space. The use of FFT procedures to solve Eqs. (1a) and (1c) avoids the use of spatial differencing to evaluate the Laplacian, a procedure which then requires the laborious use of matrix inversions to solve the equations. In this way the algorithm resembles ESOP [7] but is different from the PR algorithm [6]. On the other hand the Crank-Nicolson form of the net advancement algorithm [Eq. (2)] also holds for the PR algorithm [6], making possible an implicit temporal advance both for PR [6] and the present algorithm (ISOP), but differs from the net ESOP [7] advancement algorithm, which is explicit and thus not well suited for Coulombic problems.

III. Theoretical results

Here we study He^{++} on H charge-exchange collisions, for which experimental [12, 13] and previous theoretical results [14-17] exist and for which there is disagreement between the theoretical results of Hose [17] and those of other authors [14-16]. The calculations of the other authors [14-17] are based on time-dependent close-coupling theory, in which the Schroedinger equation is solved by expanding the wave function in a basis set. Not surprisingly the source of the disagreement derives from how such basis sets should be chosen. The TDSE approach, in the sense that the numerical solution in principle contains the complete set of states and automatically describes the translation of the electron in the directions of the target atom or projectile, is well suited to resolve such disagreements.

A classical straight-line trajectory is used to describe the heavy-particle motion, making the interaction potential time dependent. Eq. (1b) implies that this potential should be split between the advanced and retarded solutions; however this procedure prevents the factorization of the Hamiltonian and the

wave function difference which is necessary for the truncation error to be of order dt^3 in the formal Crank-Nicolson net advancement algorithm [Eq. (2)]. Thus it has been found to lower the accuracy of the calculation. For example at a dt of 0.05 (which is used for most of the calculations, with smaller dt's used on selected runs to confirm the accuracy of this choice) we have found that energy is seriously unconserved. It is also likely however that the loss of accuracy caused by this procedure is due to the evaluation of the ratio of the singular potential [Eq. (1b)] at two slightly different time points. (The potential is cutoff near the singularity using the procedure described in the Appendix.) Therefore we chose to evaluate the potential at the midpoint of dt, thereby ensuring second-order accuracy [Eq. (2)] and conservation of energy to high accuracy on our temporal grid. Trial runs in which V is evaluated at the advanced or retarded times provided empirical evidence of an insensitivity of the results to where V is evaluated within the interval dt so long as it is evaluated at a single point and not split between the advanced and retarded points.

The spatial grid used in most of the runs consisted of a

rectangular box of dimension 24x24x48 a.u., whose height is in the direction (along z) of the heavy-particle trajectories with 80x80x160 grid points respectively; selected runs used to confirm the accuracy of this choice used a box dimension of 24x24x72 a.u. and 80x80x240 grid points respectively. The target atom and projectile ion are positioned at initial time equidistant from the positive and negative z-axes respectively. The initial atomic wave function, which is an eigenfunction of the Hamiltonian outside the interaction region, is written using the geometric midpoint of the nuclei as the electron's reference frame [18],

$$\psi_{1s} = [\varphi_{1s} e^{-i(\varepsilon_{1s} + v^2/8)t}] e^{-i\frac{v}{2}z} , \qquad (3)$$

where v is the relative collision velocity.

The target atom is centered in the right-hand grid position as already mentioned. As time progresses atom and ion move to the left and right respectively and pass each other at z = 0 and at the temporal point $t_{max}/2$, which is the center of the interaction region, at impact parameters from b=0 to b=9 at intervals of db=0.75. This spacing in b does not fully resolve the oscillating

behavior at the smaller b's at the lower velocities (v= 0.2 and 0.3) is not fully resolved; however we find that a Δb 0f 0.75 is sufficient to resolve the peak to valley versus b and thus is expected to be of acceptable accuracy for the integrated cross section.

The line perpendicular to z, whose distance is the impact parameter, is directed toward two opposite corners of the box, which is a geometrical arrangement which keeps the nuclear centers as far as possible from the grid boundaries for a given impact parameter. At t_{max} the channel amplitudes are calculated from the overlaps of the numerical wave function and the channel eigenfunctions centered to the right (projectile) and left (target) of the interaction region. For example the complex conjugate of Eq. (3), centered on the left-hand side of the interaction region at t_{max}, is the target 1s channel eigenstate. The squared moduli of the amplitudes are the probabilities as a function of impact parameter P(b) for populating the states, and the cross section is calculated from 2π b P(b) integrated over b from zero to b_{max}.

The part of the electronic wave function which reaches the grid boundaries is absorbed by means of a negative imaginary part $-i\gamma$

added to the potential near the boundary edge, where γ is ramped spatially to a maximum value $\gamma_{max} = 2$ at the boundary edge using a Gaussian ramp function exp[-(i/3)**2], where i = 0, 1, 2..... from the edge, until the strength of the potential reaches 0.01, at which point it is taken to be zero. We carried out tests for larger, smaller, and smoother absorptive potentials; these tests indicated that our choice is adequate in the sense that we do not observe reflection at the boundary walls. The existence of boundaries at the sides of the grid box in the numerical TDSE approach requires care that the electronic quantum states of the target and projectile are far enough away from the boundaries not to be significantly absorbed. We have assured ourselves that the n=2 and n=3 levels of the projectile are in this category so that we can reliably report their cross sections as shown in Figs. 1-3.

Fig. 4 shows the ionization cross section. We calculate the probability for ionization from the decay of the norm of the wave function due to absorption through the boundaries. For impact parameters between 8 and 9 we observe that b $P(b)_{ion}$, which is

small, begins to show a slight rise, an effect which we attribute to the beginning of the absorption of the projectile n=3 and the target n=2 bound orbitals. Of course all bound orbitals of higher n, although they are weakly populated, will contribute to what we have called the "ionization" cross section; the small velocity results of Fig. 4 illustrate this point in that our data points do not go to zero with the other data. The error bars on our data reflect our estimate that the uncertainty in our ionization cross section is about 10%, with the minimum of the error bars measuring the spurious contribution of bound orbitals (note that these minima agree with the other data at small velocity) and the maximum reflecting the dependence of the model on box size and choice of temporal and spatial grid steps. However we believe that the uncertainty in the bound-state cross sections reported in Figs. 1-3 can reasonably be expected to be less than 10%.

In Figs. 1-3 we compare our results with experimental [12] and other theoretical [14-17] results for capture into the n=2 and n=3 states of He^+. In Fig. 4 we compare against experimental [13] and other theoretical [16-17] results for target ionization. The previous

theories are described as follows. Errea et al. [14] expand in a molecular basis with a common translation factor optimized by a procedure described by them. Fritsch [15] expands in an atomic basis set with translation factors. Winter [14] expands in a triple-centered atomic basis set with translation factors. Hose [17] expands in a molecular basis set without translation factors, arguing that the channel amplitudes can be decoupled in the asymptotic region from a diagonalization of a temporal weighted average of channel propagators which he had previously proposed [19].

One notes that Hose's [17] calculation underestimates the n=2 cross section (Fig. 1) and overestimates the n=3 cross section (Fig. 2) compared with the measured cross sections [12] and the theoretical cross sections calculated by others [14-16] and by the present authors. On the other hand all of the theoretical cross sections show good mutual agreement for the sum of the n=2 and n=3 cross sections (Fig. 3) due to the tendency of Hose's low and high results for n=2 and n=3 respectively to be mutually compensatory. We believe that our results help resolve the theoretical disagree-

ment in favor of the theories which use translation factors [14-16].

IV. Summary and conclusions.

We have presented and implemented an implicit FFT method for solving the Schroedinger equation in the time and three spatial dimensions. The method is applied successfully to charge exchange and ionization in He^{++} on H collisions. Generally we believe that the numerical TDSE method, in the sense that the solution spans the complete spectrum of electronic states, including translation effects, for any instantaneous arrangement of the nuclei, helps to eliminate any element of subjectivity which might somehow persist in methods which require judgemental decisions in the selection of a basis set. Indeed the theoretical disagreement noted above is fundamentally of this character. To be sure the numerical solution has its own set of problems such as the absorbing boundary artifice and, more seriously, the need in multi-electron problems to represent the potential using mean-field approximations. The latter point will be the subject of future work.

Appendix

A uniformly spaced cartesian grid with points centered about the Coulomb singularity defines its own cutoff of the potential. However one can see that an arbitrarily positioned gridwork can create a large error in the numerical representation of the potential operator if a grid point lies too near the singular point. We make the following argument for the modification of the Coulomb field when used with the FFT grids. Consider the integral over a spherical volume of radius R centered about the singular point of the potential:

$$\int d^3r\, 1/r = 4\pi \int_0^R r^2\, dr\, 1/r = 2\pi R^2 \qquad \text{(A1)}$$

If we equate the spherical volume to the volume of a rectilinear cartesian volume element assuming that the increments are similar in x, y, and z, we find:

$$\begin{aligned} &\tfrac{4}{3}\pi R^3 = (dx)^3, \\ &R = dx\,(3/4\pi)^{1/3}. \end{aligned} \qquad \text{(A2)}$$

If we now equate the integral over the singularity in Eq. (A1) to the trapezoidal value of that integral with a cutoff of r_x imposed in the Coulomb potential , we have

$$2\pi R^2 = (1/r_x)\,(dx)^3, \qquad \text{(A3)}$$

from which we can now solve for r_x using the value of R from Eq.(A2):

$$r_x = (2/9\pi)^{1/3}\, dx \approx 0.414\, dx. \qquad \text{(A4)}$$

The Coulomb potential is simply evaluated with $r = \max[r, r_x]$) . The value of dx in Eq.(A4) is the spatial grid increment, of course. One notes that r_x is less than half of the space increment so that the cutoff is immaterial for grids centered symmetrically about the singularity.

Acknowledgements. The authors wish to thank Gabriel Hose and Charles Cerjan for helpful discussion. This work was performed under the auspices of the U. S. Department of Energy by Lawrence Livermore National Laboratory under Contract No. W-7405-ENG-48 and of Sandia National Laboratory under Contract No. DE-AC04-94AL85000

References

1. V. Maruhn-Rezwani, N. Grun, and W. Scheid, Phys. Rev. Lett. **43**, 512 (1979).

2. K. R. Sandhya Devi and S. E. Koonin, Phys. Rev. Lett **47**, 27 (1981).

3. K. C. Kulander, K. R. Sandhya Devi, and S. E. Koonin, Phys. Rev. A **25**, 2968 (1982).

4. Ch. Bottcher, Phys. Rev. Lett. **48**, 85 (1982).

5. N. Grun, A. Muhlhans, and W. Scheid, J. Phys. B **15**, 4043 (1982).

6. D. W. Peaceman and H. H. Rachford, J. Soc. Indust. Appl. Math. **3**, 28 (1955).

7. M. D. Feit, J. A. Fleck, Jr., and A. Steiger, J. Comput. Phys. **47**, 412 (1982).

8. J. C. Wells, D. R. Schultz, P. Gavras, and M. S. Pindzola, Phys. Rev. A **54**, 593 (1996).

9. A. Kolakowska, M. S. Pindzola, F. Robicheaux, D. R. Schultz, and J. C. Wells, Phys. Rev. A **58**, 2872 (1998).

10. A. Burke Ritchie and M. E. Riley, Sandia National Laboratories Technical Report, SAND97-1205, June 1997 (available on the internet webpage at http://www.sandia.gov/library.htm.

11. B. Ritchie, P. Dykema, and D. Braddy, Phys. Rev. E **56**, 2217 (1997).

12. D. Ciric, C. Dijkkamp, E. Vlieg, and F. J. de Heer, J. Phys. B **18**, 4745 (1985).

13. M. B. Shah, D. S. Elliott, P. McCallion, and H. B. Gilbody, J. Phys. B **21**, 2455 (1988); M. B. Shah, H. B. Gilbody, J. Phys. B **14**, 2361 (1981).

14. L. F. Errea, J. M. Gomez-Llorente, L. Menez, and A. Riera, J. Phys. B **20**, 6089 (1987).

15. W. Fritsch, Phys. Rev. A **38**, 2664 (1988).

16. T. G. Winter, Phys. Rev. A **37**, 4656 (1988).

17. G. Hose, Phys. Rev. A **56**, 1364 (1997).

18. M. E. Riley, Phys. Rev. A **7**, 626 (1973).

19. G. Hose, Phys. Rev. A **51**, 2199 (1995).

Figure Captions

Fig. 1. Cross section in a. u. (i. e. square bohr) for capture into the n=2 level of the projectile versus collision velocity in a. u.

Fig. 2. Cross section in a. u. (i. e. square bohr) for capture into the n=3 level of the projectile versus collision velocity in a. u.

Fig. 3. Cross section sum in a. u. (i. e. square bohr) for capture into the n=2 and n =3 levels of the projectile versus collision velocity in a. u.

Fig. 4. Cross section for ionization of the target in a. u. (i. e. square bohr) versus collision velocity in a. u.

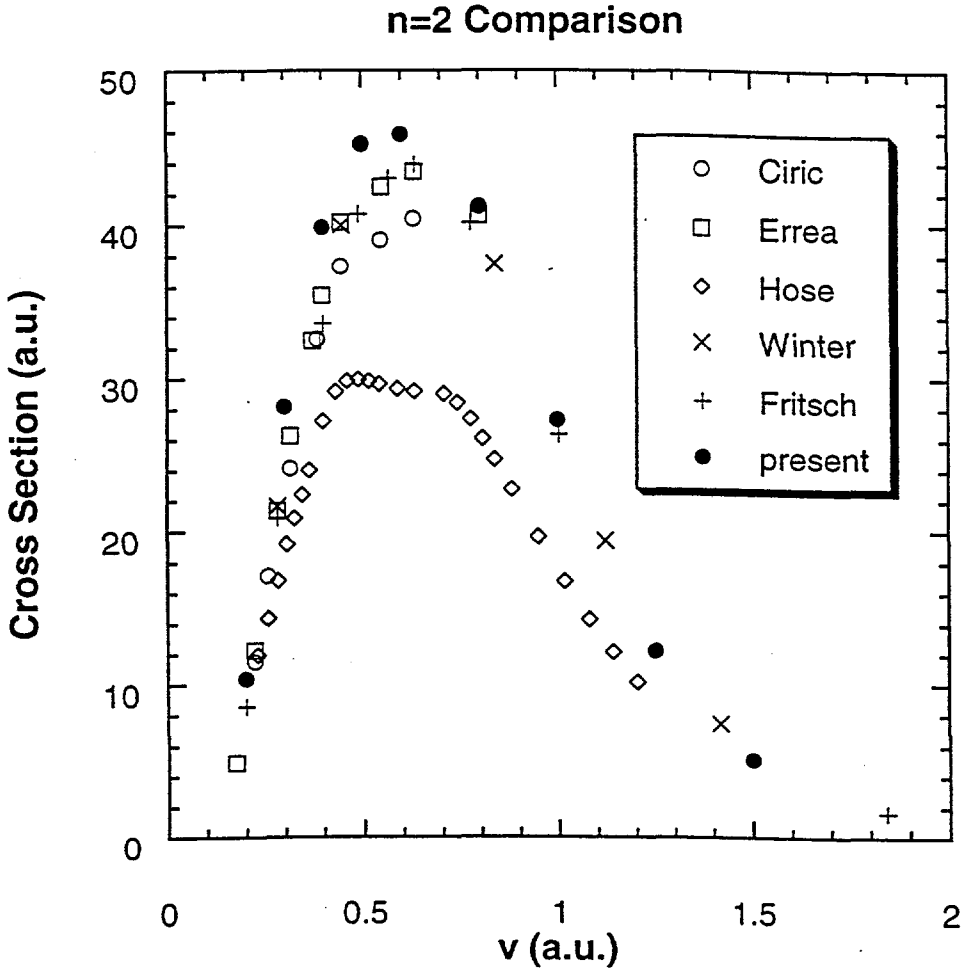
n=2 Comparison
Cross Section (a.u.)
v (a.u.)
0
10
20
30
40
50
0
0.5
1
1.5
2
Ciric
Errea
Hose
Winter
Fritsch
present

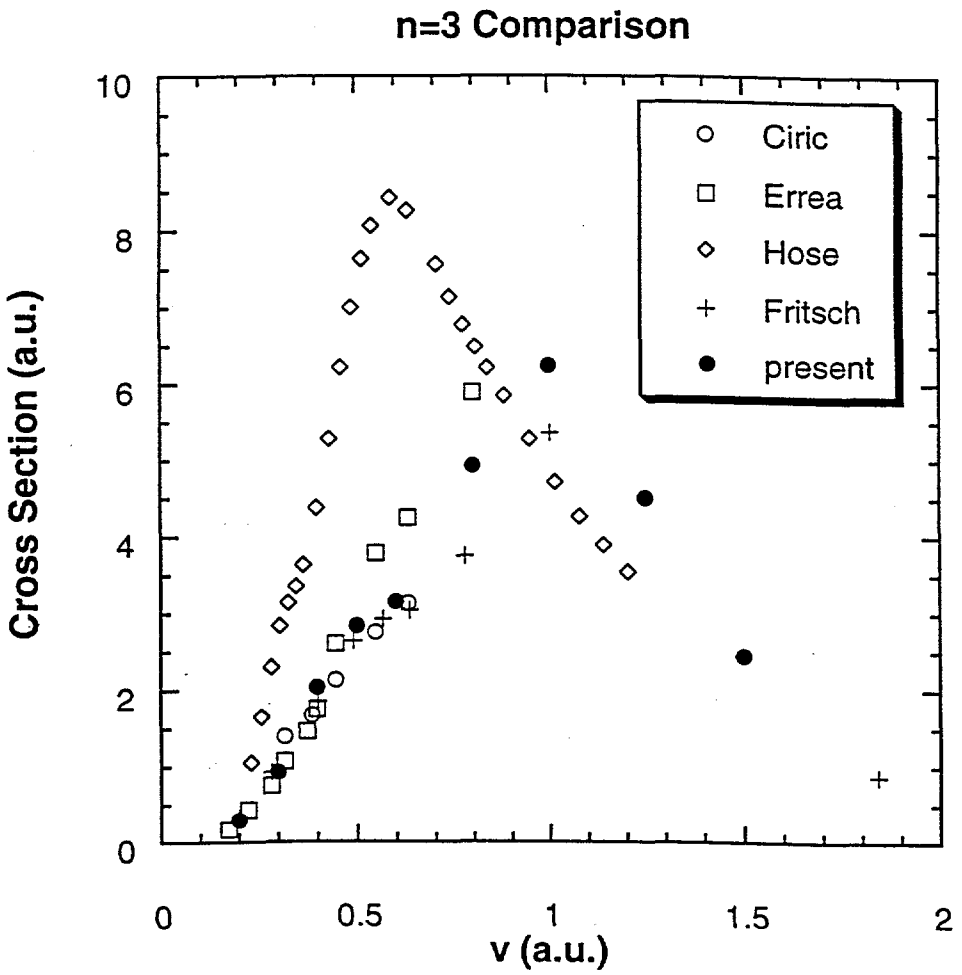
n=3 Comparison
Cross Section (a.u.)
v (a.u.)
0
2
4
6
8
10
0
0.5
1
1.5
2
Ciric
Errea
Hose
Fritsch
present

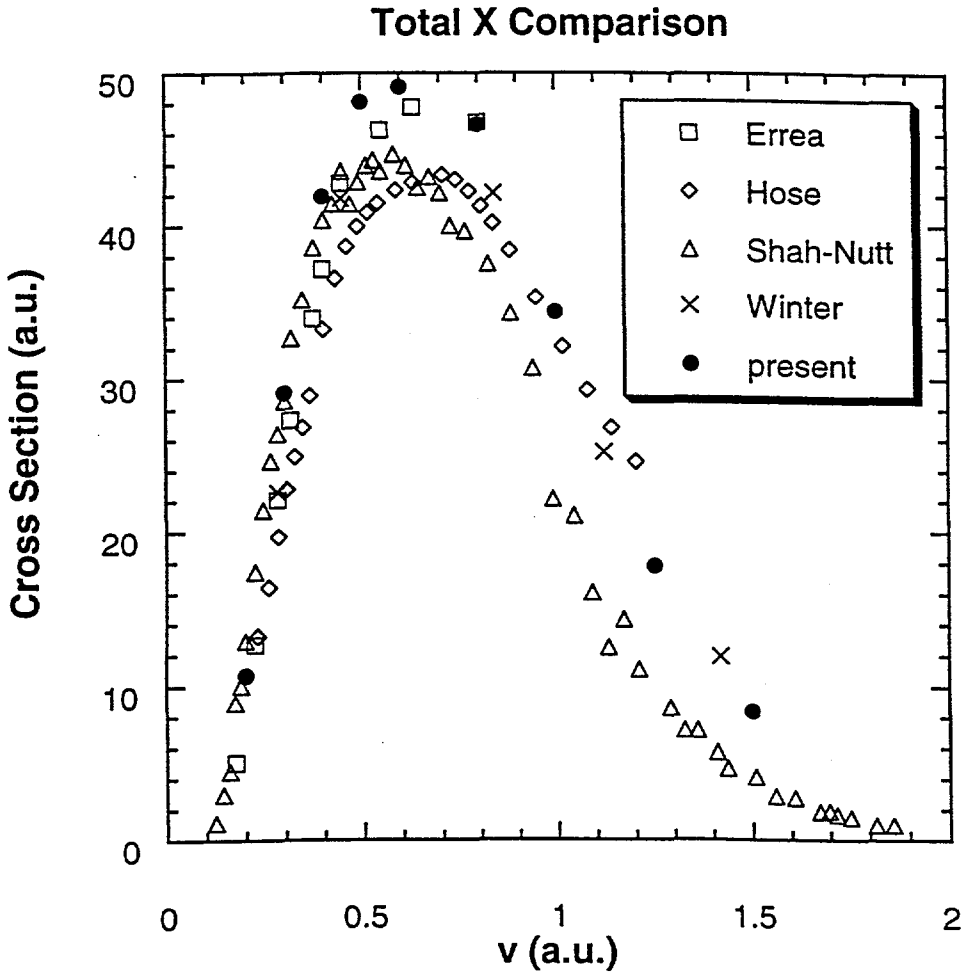
Total X Comparison
Cross Section (a.u.)
v (a.u.)
0
10
20
30
40
50
0
0.5
1
1.5
2
Errea
Hose
Shah-Nutt
Winter
present

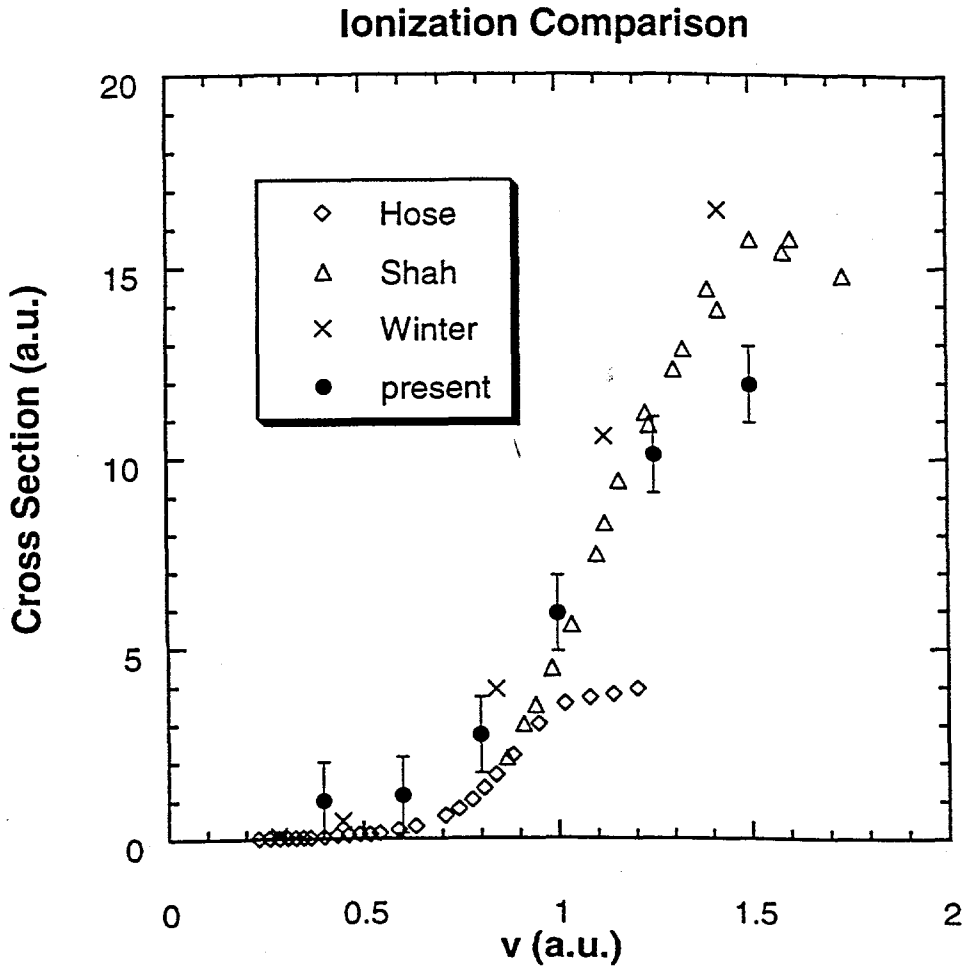
Ionization Comparison
Cross Section (a.u.)
v (a.u.)
Hose
Shah
Winter
present
0
5
10
15
20
0
0.5
1
1.5
2